FLUORESCENCE STUDIES OF

TRIS (2,2'-BIPYRIDINE) RUTHENIUM(II)

IN THIN CLAY FILMS

By

Samuel James Salamone

* * * * * * * *

Submitted in partial fulfillment

of the requirements for

Honors in the Department of Chemistry

UNION COLLEGE

June, 2000

ABSTRACT

SALAMONE, SAMUEL   Fluorescence studies of tris (2,2'-bipyridine) ruthenium(II) in thin clay films. Department of Chemistry, June 2000.

Because of their rich intercalation chemistry and ability to enhance the thermal stability of the included guest, layered silicate clays are excellent hosts for the fabrication of organic/inorganic nanocomposites. Composites of hectorite and tris(2, 2'-bipyridine) ruthenium(II), $Ru(bpy)_3^{2+}$, have attracted attention owing to their potential applications as glucose and oxygen based chemical sensors. Previous studies on the fluorescence behavior of $Ru(bpy)_3^{2+}$ complexes in aqueous colloidal clay suspensions have shown enhanced emission traces. We report here the first study of the fluorescence responses of $Ru(bpy)_3^{2+}$ exchanged thin clay films. Variation of guest concentration and exposure time and choice of host clay framework have significant impacts on the resultant fluorescence response. These parameters may be used to optimize the observed emission and excitation spectra of organic/inorganic nanocomposites. Powder X-ray diffraction (XRD) was used to verify intercalation of the $Ru(bpy)_3^{2+}$ into the clay framework. These studies may enhance our understanding of fundamental host-guest interactions, chiral templating, and the intercalation process.

ACKNOWLEDGEMENTS

I would first and foremost like to acknowledge God for giving me the strength, wisdom, and courage to get through the first 21 years of my life successfully and for helping me deal with whatever I was dealt.

Secondly, I would like to thank my family for their undying love and support, especially in the difficult times when I felt lost in my way. I would also like to thank all my friends who have made the journey through life all the easier and more enjoyable. I thank all of the teachers that I have had, from pre-school through high school. The knowledge that you gave me has served me well.

Finally, I send my sincerest appreciation to the entire faculty and staff of Union College. I appreciate all that you have done for me throughout my time here. Specifically, I would like to thank Prof. Michael Hagerman, for putting up with me for three years and for being a friend as well as an advisor, and Prof. and Mrs. Charles Scaife, who have been like a second set of parents to me.

Table of Contents

Table of Figures

Table of Tables

1. Introduction

A new discipline has emerged at the interface between materials science, inorganic and organic chemistry. This discipline includes the study of inorganic/organic hybrid nanocomposites. These materials are formed using an inorganic host framework and an organic or organometallic guest. Investigation of the chemical factors that control the inner architecture of solids and exploiting these factors to rationally design advanced materials that meet the increased performance levels of modern technological applications has become an important part of this discipline. The composites are interesting because they take advantage of the useful properties of each of their components. The guest usually provides the desired characteristic of the material. In our case, the property of interest is fluorescence. The host provides a stable framework that serves as a support for the guest and affords a multitude of different forms and applications. The guest molecules in these composites enter the host through a process known as intercalation, which is the reversible insertion of a guest into a host material while maintaining the structural features of the host.[1] An example of a general intercalation system is shown in **Figure 1-1**.
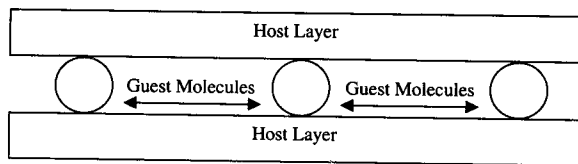
Figure 1-1: General Model of Intercalation

1

Much work has already been done in the area of inorganic/organic hybrid nanocomposites. Pinnavaia[2] has discussed uses of pillared lamellar solids (e.g. smectite clays, such as montmorillonite and hectorite) and layered double hydroxides, (composites of the form $[M_{1-x}^{II}M_x^{III}(OH)_2][A^{n-}]_{x/n} \cdot zH_2O$, where A^{n-} is the gallery anion, and M^{II} and M^{III} are divalent and trivalent cations, respectively). Inorganic, "pillar" molecules (e.g. $Al_{13}O_4(OH)_{24}(H_2O)_{12}^{7+}$ and other metal oxides) were introduced between layers of these inorganic solids. The pillars produce vertical spaces between the rigid layers of the host, as well as lateral spaces between the pillar molecules. It has also been shown that molecules with organic tails (e.g. $P-C_6H_5-C_6H_5-P$, which attaches to the clay surfaces by binding at its phosphorous atoms and bridges the gap between layers with its phenyl rings) can be used as pillaring agents.[2] These types of pillars make the space between layers hydrophobic and able to accept other organic molecules. These nanocomposites have proven to be very useful in heterogeneous catalysis and the production of petroleum products and biproducts.[2]

Giannelis[3] and Schöllhorn[4] have also investigated the usefulness of layered silicates (e.g. hectorite) as host materials. It was demonstrated that guest molecules, such as ethylenediamine-functionalized buckminsterfullerene display enhanced thermal stability when incorporated between layers of the clays.[3,4] The hectorite has also been shown to be useful in the catalysis of polymerization processes. The clay was exchanged with redox active cations, such as Cu^{2+}, then monomers, such as aniline and pyrrole were incorporated, and polymerization ensued.[3,4] In another approach toward hybrids of clay and polymer, polymers (not monomers) were directly inserted into the inter-layer spaces[3,4].

Zeolites have been explored as potential hosts, as well. These are inorganic structures that have, "cages," rather than inter-layer regions, into which guest molecules can be inserted. Turbeville,[5] DeWilde,[6] and Lainé[7] have all explored zeolites in colloidal suspension as host materials for the fluorescently active, organometallic, Tris (2,2'-bibyridine) Ruthenium(II) or $Ru(bpy)_3^{2+}$.

A primary application of all of these hybrids is in chemical sensing. A wide variety of sensors have already been developed.[8-12] Ammonia sensors have been studied that use $Zn(O_3PC_6H_5) \cdot H_2O$ as a host into which ammonia and amines can be incorporated and detected.[8] Humidity sensors have been explored using hectorite clay deposited on interdigitated arrays[9] and using hectorite clay and organic polymers.[10] Biomolecular sensors have been studied using polypyrrole, polythiophene, and polyaniline conducting polymers.[11] Glucose sensors have also been devised using montmorillonite clay and a ruthenium organometallic guest.[12]

We are interested in developing a nanocomposite that will have potential applications in glucose sensing. Glucose is involved in promoting the oxidation of $Ru(bpy)_3^{2+}$, which results in the quenching of its luminescence response. The host framework that we have chosen is hectorite and the guest molecule is $Ru(bpy)_3^{2+}$. $Ru(bpy)_3^{2+}$ enters the clay structure through intercalation. Some work has already been done with similar composites using the ruthenium polypyridyl complex $Ru(phen')_3^{2+}$ and poly(p-phenylene vinylene) films. It has shown that these device quality composites can be produced.[13] However, we report here the first study of the emission properties of $Ru(bpy)_3^{2+}$ / hectorite nanocomposites.

3

1.1 Tris (2,2'-bipyridine) Ruthenium (II) or Ru(bpy)$_3^{2+}$ and Fluorometry

Ru(bpy)$_3^{2+}$ is a complex with a Ruthenium atom surrounded by three bidentate bipyridine ligands in an octahedral arrangement. The structure can be seen in **Figure 1.2**.
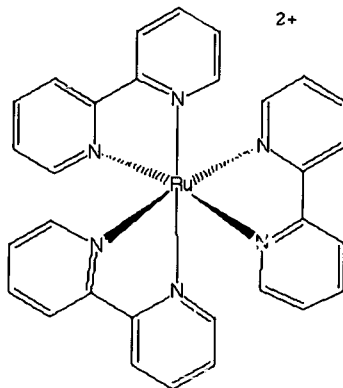
Figure 1.2: Structure of Ru(bpy)$_3^{2+}$

The reason that we have chosen to use Ru(bpy)$_3^{2+}$ as the guest for our composites is its intense luminescence properties. Two types of fluorescence measurements, excitation and emission, are used. Previous work has shown that this complex is excited by 460 nm light.[14] When it relaxes back down to the ground state, it emits 610 nm light. This emission is measured using a fluorometer. The instrument excites the sample with the proper radiation and the sample relaxes back down to its ground state. Upon relaxation, the sample emits radiation, that is detected by the detector of the instrument. The detector measures the intensity of emission over a range of wavelengths, thus a peak

4

is observed at the specific emission wavelength(s) of the sample. The intensity of that peak is directly proportional to the number of photons that reach the detector. This type of fluorometry is known as emission fluorometry. Alternatively, the fluorometer can be set to measure the intensity of emission at one specific wavelength, while exciting the sample over a range of wavelengths. In this case, a peak is observed at the specific excitation wavelength(s), that results in the most intense emission at the given wavelength. This type of fluorometry is known as excitation fluorometry.
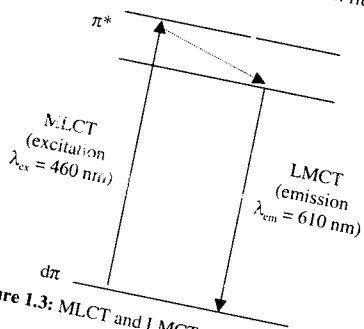
Figure 1.3: MLCT and LMCT states in Ru(bpy)$_3^{2+}$

The excited state of the Ru(bpy)$_3^{2+}$ has been attributed to the metal-to-ligand (molecular orbital of mostly d character, dπ, to the anti-bonding pi molecular orbital, $\pi*$) charge-transfer (MLCT) state.[15,16] This excitation and subsequent emission is represented in **Figure 1.3**. Upon exposure to 460 nm light (excitation), an electron in the molecular orbital of mostly d-character of the ruthenium (metal) is transferred to the $\pi*$ molecular orbital of primarily bipyridine (ligand) character. The electron then undergoes intersystem crossing to give it a lower energy. When it finally relaxes back down to the
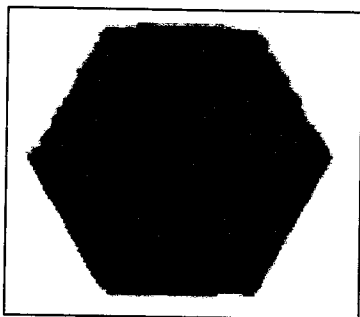
Figure 1.4: Ru(bpy)$_3$$^{2+}$/Zn-hectorite under a ultraviolet lamp

An interesting phenomenon, called quenching,[6] occurs in the emission patterns of Ru(bpy)$_3$$^{2+}$ when the concentration increases. Contrary to what might be predicted intuitively, the emission intensity actually decreases with increasing concentration. Two possible explanations for this anomalous trend have been suggested. The first explanation is that, since molecules of the complex get closer together as concentration increases, resonance transfer of excitation energy from one molecule to another can occur[6]. This would decrease the emission intensity. The other explanation is that upon increasing concentration, Ru(bpy)$_3$$^{2+}$—Ru(bpy)$_3$$^{2+}$ interactions also increase, causing a disproportionation reaction that decreases emission intensity[5] (See **Scheme 1.1**).

$$2Ru(bpy)_3^{2+}{}_{(aq)} \longrightarrow Ru(bpy)_3^{3+}{}_{(aq)} + Ru(bpy)_3^{+}{}_{(aq)}$$
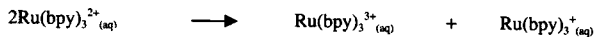
Scheme 1.1: The electron transfer that is potentially responsible for the self-quenching observed at high concentrations of $Ru(bpy)_3^{2+}$

Therefore, at low $Ru(bpy)_3^{2+}$ concentrations, the emission intensity is greater because the extent of interaction between $Ru(bpy)_3^{2+}$ molecules is not significant enough to drive the resonance transfer or the electron transfer. Increasing $Ru(bpy)_3^{2+}$ concentration adds more fluorophore and increases the emission intensity until the $Ru(bpy)_3^{2+}$—$Ru(bpy)_3^{2+}$ interactions become significant enough to drive the transfers. At this point a decrease in emission intensity is observed.

1.2 Hectorite and X-Ray Diffraction

Hectorite is a layered smectite-type clay, meaning that its unit cell consists of a 2:1 ratio of tetrahedral and octahedral layers. The tetrahedral sheets are comprised of Si^{4+}, while the octahedral sheets are cations of Al^{3+}, Mg^{2+} and Li^+. A structure of Na-hectorite is shown in **Figure 1-5**. Both layers share oxygen at their vertices. However, when the framework Si^{4+} ions are replaced with ions of lesser positive charge (i.e. Al^{3+}), the clay develops a net negative charge. This negative charge must be balanced by adding cations to the clay.[16,13]

The unit cell of the clay also includes an intergallery region. This region exists between tetrahedral-octahedral-tetrahedral layers. The intergallery region contains water and the cations that balance the excess negative charge in the layers (the hectorite that we started with contained Na^+ in the intergallery region, and is, therefore, called Na-

7

hectorite). It is into this intergallery region that we initially proposed that the Ru(bpy)$_3$$^{2+}$ would be inserted. However, it could also deposit on the surface of the clay or between the edges of unit cells.[14,13]

The hectorite (along with the alternative host, MCM-41) was analyzed using a technique known as X-ray diffraction (XRD). XRD provides the d-spacing of the substance analyzed. The d-spacing is the distance from the top of one tetrahedral layer, through the intergallery region and to the top of the other tetrahedral layer (see **Figure 1-5**).

Figure 1-5: Structure of Na-hectorite

In XRD, electrons are boiled off of a tungsten source and accelerated at cobalt, knocking out inner core electrons of the cobalt. These electrons must be replaced, so

electrons in higher energy levels drop down to the lower, vacant energy levels. In the process, they radiate energy (X-rays). An iron filter separates this radiation such that only radiation of 1.790 Å wavelength reaches the sample. The sample rotates and the X-rays strike it at an angle (θ) that is valid from 0°-60°. However, since the layers of the sample are repetitive at some θ angles, the X-rays constructively interfere with each other and at other angles they destructively interfere. Therefore, the silicon detector will detect X-ray radiation only if it is reflected into it at specific θ angles (see **Figure 1-6**[17]).

Figure 1-6: Schematic representation of X-rays reflecting off a clay sample at angle θ (after Chang[17])

The angle of reflected radiation is related to d-spacing by Bragg's Law[18]:

$$n\lambda = 2d(\sin\theta)$$

Where n is an integer, λ is the wavelength of the radiation (1.790Å), d is the distance between layers as shown in **Figure 1-6**, and θ is the incident and reflected angle of the X-rays off the sample.

9

An important feature of this layered clay is that its intergallery region is expandable. That is, its dimensions can adapt to the dimensions of the guest molecule.[4] Therefore, the space can expand to intercalate molecules, such as $Ru(bpy)_3^{2+}$, that are bigger (diameter 12.1 Å)[7] than the normal size of the region (about 6 Å).

Hectorite has been chosen as the ideal guest framework for our experiments for two main reasons. Firstly, the iron content in hectorite is low. This is important because iron has been shown to significantly quench $Ru(bpy)_3^{2+}$ emission[14,19,20]. Secondly, we have had much success in casting hectorite into thin films once the Na^+ ions have been exchanged with other cations such as VO^{2+}, Cr^{3+}, Mn^{2+}, Fe^{3+}, Co^{2+}, Ni^{2+}, Cu^{2+}, and Zn^{2+}.[21] The hectorite films will provide a rigid structure for the $Ru(bpy)_3^{2+}$. These new nanocomposites should be more easily incorporated into device structures.

1.3 Mesopores and MCM-41

Mesoporous materials are potentially useful alternative host frameworks for our nanocomposites. They are rigid pore systems that can intercalate guest molecules into their pores[4,22,23] (see **Figure 1-7**[22]) One such mesopore is MCM-41. This host forms a hexagonal array of pores that have been synthesized to range in size from 15 to 100 Å in diameter[23] (see **Figure 1-8**[23]). We have successfully performed the complicated synthesis of this material. Preliminary studies of loading MCM-41 with dye molecules has begun.

Figure 1-7: Schematic diagram of intercalation and subsequent polymerization of aniline in the pores of MCM-41 (after Wu, et al.[22])

Figure 1-8: Transmission electron micrographs of several MCM-41 materials of varying pore diameter (after Beck, et al.[23])

1.4 Goals

Much work has been done in the study of $Ru(bpy)_3^{2+}$ in clay systems, but only in colloidal suspension[19,20]. It has been shown that these colloidal composites enhance the emission intensity of the luminescent complex. However, little work has been done to transform these composites into the useful solid state. Therefore, this research has focused on this end and the optimization of the luminescent response of $Ru(bpy)_3^{2+}$ in hectorite films through the control of the amount of complex intercalated and transition metal exchanged film used. We also provide fundamental studies of the intercalation processes.

2. Experimental

This research began with the synthesis of Tris[2,2'-bipyridine] Ruthenium (II) chloride hexahydrate. We then exchanged Na-hectorite with zinc (II) and copper (II) cations and cast films, both free standing and on fused quartz. In order to optimize luminescence in the nanocomposites, we proceeded to expose the films to the complex, varying both the amount of $Ru(bpy)_3^{2+}$ intercalated and the type of transition metal exchanged into the hectorite. These composites were then ae. nalyzed using excitation and emission fluorometry as well as powder X-ray diffraction. We also successfully synthesized the mesoporous host, MCM-41.

2.1 Synthesis of $Ru(bpy)_3Cl_2 \cdot 6H_2O$

$Ru(bpy)_3Cl_2 \cdot 6H_2O$ was synthesized as specified by Broomhead, et al.[24] The overall reaction for the process was:

$$RuCl_3 + 3C_{10}H_8N_2 \xrightarrow{\quad NaH_2PO_2/H_2O \quad} [Ru(C_{10}H_8N_2)_3]Cl_2 \cdot 6H_2O$$

The only adjustment that was made to the procedure was that all of the reagent quantities were doubled, so as to increase yield. Therefore, 0.8 g of dried $RuCl_3$ was refluxed with 1.8 g of 2,2'-bipyridine, 80 mL of water, and 4 mL of freshly prepared sodium hypophosphite solution (1.66 g of NaH_2PO_2 in 4 mL of 31% phosphinic acid). The resultant solution was filtered and 25.2 g of KCl was added to the filtrate. The crude precipitate and the solution was boiled and then left to cool. The refined, red, plate-like crystals were then filtered off, washed four times with 5 mL of ice-cold 90% acetone solution and then 60 mL of ice-cold acetone. The final yield was about 1.5 g.

2.2 Synthesis of Exchanged Hectorite Films

Synthesis of the exchanged hectorite films was carried out as indicated by Eastman and coworkers[25] with a few minor changes. The salt solutions used were 0.5 M $Zn(NO_3)_2$ and 0.5 M $CuSO_4$. Each exchange used 0.4 g of Na-hectorite powder for every 100 mL of salt solution. The powder and solution were allowed to stir for one week. After the exchange, the clay from the $CuSO_4$ solution was washed and centrifuged until the supernatant produced a negative test for SO_4^{2-} (i.e. addition of $BaCl_2$ yielded no precipitate). The clay from the $Zn(NO_3)_2$ solution was washed and centrifuged five times. Films were then cast by allowing a suspension of the clay to dry either free standing in a polystyrene weigh boat or on fused quartz. In the case of the weigh boat, the resultant films could be removed, cut, and mounted on various supports. In the case of the fused quartz, the films were much thinner and strongly bound to their support.

2.3 Synthesis of $Ru(bpy)_3^{2+}$/Hectorite Composites

After synthesizing the host clay and guest complex, approximately 0.7 mL of $Ru(bpy)_3^{2+}$ solution of the desired concentration was poured on the films, such that the whole film was immersed. Solution concentrations of 1×10^{-5} M, 2×10^{-5} M, 1×10^{-4} M, 1×10^{-3} M, 1×10^{-2} M $Ru(bpy)_3^{2+}$ were used. The solution and film were left to stand for the desired amount of time, after which the solution was either poured or pipetted off. Exposure times of 1 s, 10 s, 30 s, 1 min, 45 min, 1 hr, 3 hr, and 6 hr were used. Studies were also performed where the excess $Ru(bpy)_3^{2+}$ on the surface of the clay was washed off with deionized water.

2.4 Synthesis of MCM-41

The synthesis procedure for MCM-41 was a very complicated process provided by Davis[26]. All of this synthesis was carried out in nalgene bottles and centrifuge tubes (except for the Parr bomb reactor and the aluminum boats) so as to avoid the incorporation of silicon inherent in glassware. We started by combining 29.2 g of Cetyltrimethylammonium chloride (CTACl), a templating agent, and 0.83 g of ammonium hydroxide (NH_4OH) while stirring. Next, we dissolved the solution in 4.6 g of tetramethylammonium hydroxide (TMAOH·$5H_2O$) and added 36.62 g of tetramethylammonium silicate (TMA·2[SiO_2]). A creamy white precipitate forms and then we continued stirring for 15 minutes. At this point, most of the precipitate seemed to have dissolved. Stirring continued for 1.5 hours and a new precipitate formed. The mixture was a creamy, white, homogeneous solution. Next, we stirred in 7.5g of Cab-O-Sil (SiO_2) using a Teflon spatula. When homogenized, the solution was placed in a Parr Reactor, which was placed in a Carbolite oven (PF120 200). The oven was set to heat statically at 140 degrees Celsius for 48 hours. The resultant paste was then washed with water until neutral and evenly distributed in aluminum tube furnace boats and placed in the tube Carbolite tube furnace (HST 12/50/400) for calcination. The furnace was set such that the temperature in the furnace rose 1 degree Celsius per minute until it reached 540 degrees. The product white powder was recovered after calcination for 15 hours at 540 °C, ground up, and then the calcination was repeated. All heating in the tube furnace was done under dry, flowing air. MCM-41 synthesis follows a liquid crystal templating process.[16] Such a process is illustrated in **Figure 2-1**.[23]

Figure 2-1: Liquid crystal templating process by which MCM-41 is formed (after Beck, et al.[23])

Liquid crystal templating begins with the formation of micelles by the templating agent.[23] The nonpolar, hydrophobic tails of the templating congregate to the center of a micelle, while the polar heads aggregate to the outside. These micelles then stack on top of each other to form micellar rods. The rods naturally arrange themselves in a hexagonal array. When the polar silicate is added, it congregates to the outside of the micellar rods and coats them. The templating agent is then calcinated (burned) out and what is left is the silicate arranged in a hexagonal array of hollow tubes (pores).

2.5 Fluorometry

All fluorometry was carried out on the PTI Quantamaster Fluorometer. The photomultiplier tube operated at a voltage of 1000 V and the lamp at a power of 75 Watts. Both the excitation and emission monochromator slitwidth were 2 nm. Hectorite samples were prepared by free casting the films, exposing them to $Ru(bpy)_3^{2+}$, and then attaching them to a white index card, that was cut to fit in tne sample holder of the

fluorometer. The sample was placed at a 45° angle to the incident radiation. The setup of the fluorometer is represented schematically in **Figure 2-2**.

Figure 2-2: Schematic representation of the fluorometry setup used for this research

2.6 X-Ray Diffraction

All X-ray diffraction was done on a Phillips X-ray diffraction machine. The machine operated at a voltage of 45 keV and a current of 35 mA. Electrons are boiled off of a tungsten source and accelerated at cobalt, that then emits radiation of 1.790 Å wavelength. The sample rotates and the X-rays can strike it at an angle of 0°-60° θ. All scans of hectorite and hectorite composites with $Ru(bpy)_3^{2+}$ were carried out over an incident X-ray angle range of 1 - 40 °2θ. Each scan of MCM-41 was carried out over an incident X-ray angle range of 1 - 10 °2θ. All X-ray diffraction was done using a step size of 0.010 °2θ. The scan speed was 0.005 °2θ /s at 2.000 s per step, with a receiving slit of 0.3 mm. Samples were mounted for analysis in three different manners. MCM-41was

17

analyzed as a powder on an aluminum X-ray diffraction plate. Hectorite was either free cast as a film, exposed to $Ru(bpy)_3^{2+}$ and then attached to a fused quartz X-ray diffraction plate using double stick tape, or the film was cast directly onto a fused quartz microscope slide and then exchanged with exposed to $Ru(bpy)_3^{2+}$.

3. Results and Discussion

The fluorometry and X-ray diffraction results provide an abundance of information regarding the properties and ideal synthesis of $Ru(bpy)_3^{2+}$ exchanged hectorite films. These films support the optical activity of the $Ru(bpy)_3^{2+}$, and show high potential for the development of chemical sensors.

3.1 Fluorometry

Previous fluorescence studies have shown the enhanced fluorescence activity of colloidal suspensions of Na-hectorite and $Ru(bpy)_3^{2+}$.[20] We report here the first study of nanocomposite thin films of $Ru(bpy)_3^{2+}$/Zn-hectorite. Our $Ru(bpy)_3^{2+}$ film systems support the enhanced luminescence noted by Ghosh.[20]

3.1.1 $Ru(bpy)_3^{2+}$ Solutions

Before any study of $Ru(bpy)_3^{2+}$/hectorite systems could be performed, it was necessary to determine the fluorometric properties of $Ru(bpy)_3^{2+}$ independently. A number of $Ru(bpy)_3^{2+}$ aqueous solutions, varying in concentration were excited at a wavelength (ex λ) of 460 nm and the resulting emission spectra are given in **Figure 3.1**. Clearly, $Ru(bpy)_3^{2+}$ emitted very strongly at 610 nm.

The most intense emission was achieved in the 1×10^{-4} M solution. The smallest emission was the 1×10^{-2} M solution, with the 1×10^{-3} M solution slightly more intense. Therefore, it is clear that there is some upper threshold on the emission intensity of $Ru(bpy)_3^{2+}$. That is, very dilute solutions emit strongly and increase in intensity as

concentration increases. However, at a certain higher concentration, the emission intensity begins to drop.

Figure 3.1: Emission scans of varying concentrations of Ru(bpy)$_3{}^{2+}$ solutions (ex λ = 460 nm)

The evidence of an upper threshold is consistent with the self-quenching experienced by Turbeville, et al.[5] Upon loading Ru(bpy)$_3{}^{2+}$ into zeolites, increasing the concentration of Ru(bpy)$_3{}^{2+}$ within the zeolites resulted in decreased emission intensity. This quenching effect is detailed in section 1.1.

3.1.2 Ru(bpy)$_3{}^{2+}$ Colloidal Clay Suspensions

In 1984, Ghosh and Bard demonstrated that Na-hectorite, in colloidal suspension with Ru(bpy)$_3{}^{2+}$ solution, enhanced the emission intensity of the Ru(bpy)$_3{}^{2+}$.[20] Their experiment was duplicated in order to verify the fluorescence activity of our synthesized

20

Ru(bpy)$_3$$^{2+}$ and to ensure the accuracy of our fluorescence instrument. The resulting emission spectra are shown in **Figure 3.2**.
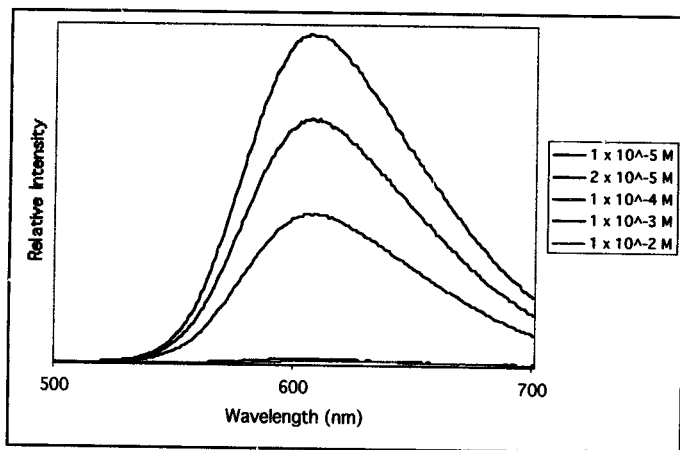
Clearly, the Na-hectorite intensified the emission of the Ru(bpy)$_3$$^{2+}$ when the two were incorporated into a colloidal suspension. The intensified emission has been attributed to an enhancement of the metal-to-ligand charge transfer.[20] The enhancement of Ru(bpy)$_3$$^{2+}$ emission in colloidal suspension suggests that similar trends may be observed if the Ru(bpy)$_3$$^{2+}$ was incorporated into cast, solid, hectorite films. These solid state complexes display more promising characteristics (compact, solid, etc.) for practical applications, including chemical sensing.

Figure 3.2: Emission scans of a Ru(bpy)$_3$$^{2+}$ solution and a colloidal suspension of Ru(bpy)$_3$$^{2+}$ and Na-hectorite (ex λ = 460 nm)

3.1.3 Mounting Support: Fluorometry of Sample Holder

The problem with studying the fluorometry of the $Ru(bpy)_3^{2+}$ exchanged films was that some sort of support was required in order to hold the film in place to be measured. Index cards served this purpose well. However, the index card led to a distorted baseline (see **Figure 3.3**).

Figure 3.3: Emission scan of a plain index card (ex $\lambda = 460$ nm)

In a normal fluorometry study of a solution, most of the excitation beam (in this case, 460 nm light) passes through the sample without ever reaching the emission detector, that is perpendicular to it. Therefore, the detector does not detect a significant portion of the 460 nm light and will not show an emission peak at this wavelength. However, in the absence of a fluorophore, the index card reflects the excitation beam directly into the detector. Therefore, the detector detects a great deal of the 460 nm light. This showed up in a very large emission peak at 460 nm. The apparent peak at 516 nm

was in fact the tail of the extremely intense peak at 460 nm. There was also a small, but very sharp peak at 565 nm, that was due to Raman scattering. The distorted baseline and Raman scattering peak must be taken into account when interpreting fluorescence data recovered from the hectorite films, particularly at low levels of $Ru(bpy)_3^{2+}$ loading.

3.1.4 Variation of Transition Metal in Hectorite Host

Since Na-hectorite does not cast quality films well, other transition metal cations have been exchanged into the hectorite for the purpose of film casting. Traditionally, Cu^{2+} has been used. However, the films resulting from Cu^{2+} exchange into Na-hectorite are a blue-green color, that may potentially interfere with the optical properties of $Ru(bpy)_3^{2+}$ by absorbing some of its emitted radiation. Therefore, we searched for another cation that casts well and produces quality films that are as colorless as possible. We have shown that Zn^{2+} fits this description. Another advantage to Zn^{2+} films as opposed to Cu^{2+} films is that Zn^{2+} is not as easily reducible as Cu^{2+}. The reduction of Cu^{2+} could lead to the oxidation of $Ru(bpy)_3^{2+}$ to $Ru(bpy)_3^{3+}$, and the emission of $Ru(bpy)_3^{2+}$ would be greatly diminished. Also, it has been shown that Cu^{2+} does quench $Ru(bpy)_3^{2+}$ emission.[16]

Initially, all studies were carried out using both Cu^{2+} and Zn^{2+} exchanged hectorite films. Zn^{2+} films were consistently determined to yield more intense emission peaks than Cu^{2+} films when exposed to the same concentration (1×10^{-3} M) and volume (0.7 mL) of $Ru(bpy)_3^{2+}$ solution for the same amount of time (see **Figure 3.4**).

Owing to the increased $Ru(bpy)_3^{2+}$ emission intensity exhibited in Zn-hectorite, relative to Cu-hectorite, all subsequent studies are reported for Zn-hectorite only. There

was a small, but sharp, peak in each of these and subsequent emission spectra located at 656 nm. We believe that this peak was due to Raman scattering.

Figure 3.4: Emission scans of Zn-hectorite and Cu-hectorite films exposed to 1 x 10^{-3} M Ru(bpy)$_3^{2+}$ solution for 1 minute (ex λ = 460 nm)

3.1.5 Variation of Ru(bpy)$_3^{2+}$ Solution Concentration

In order to find out how to achieve optimal emission from Ru(bpy)$_3^{2+}$/hectorite composites, it was necessary to know how much Ru(bpy)$_3^{2+}$ to use for each film. Examination of **Figure 3.1** shows the self-quenching effect that Ru(bpy)$_3^{2+}$ exhibits at high concentrations. Therefore, the concentration of Ru(bpy)$_3^{2+}$ in the Zn-hectorite films must not be so great that this quenching becomes significant, yet it must be great enough to achieve maximum emission intensity. **Figure 3.5** shows the emission spectra of Zn-hectorite films exposed to the same volume of varying concentrations of Ru(bpy)$_3^{2+}$ solution for 1 minute.

Figure 3.5: Emission scans of Ru(bpy)$_3$$^{2+}$-exposed Zn-hectorite (ex λ = 460 nm, exposure time = 1 minute)
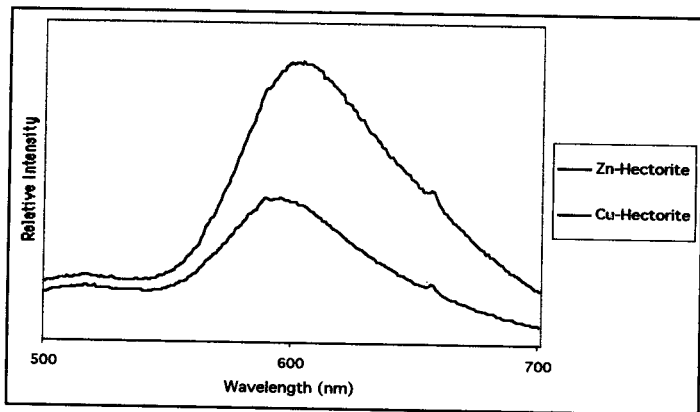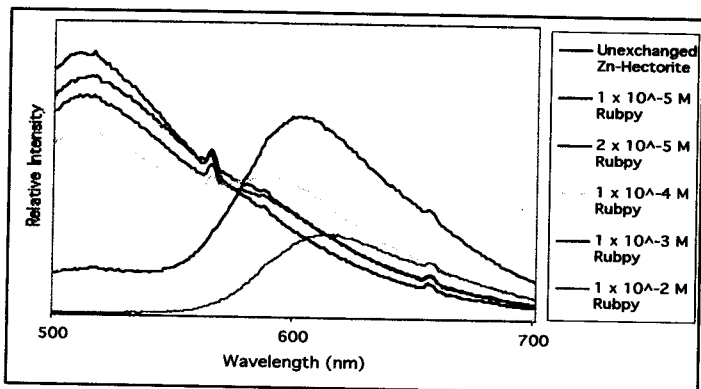
At low exposure concentrations of Ru(bpy)$_3$$^{2+}$ (i.e. unexchanged Zn-hectorite, 1×10^{-5} M, 2×10^{-5} M, and 1×10^{-4} M), two important observations could be made. First, the intensity of the Ru(bpy)$_3$$^{2+}$ signal at 610 nm was very low. Second, the distorted baseline appears to play a significant role in the spectrum. At high exposure concentration of Ru(bpy)$_3$$^{2+}$ (1×10^{-2} M), we saw a relatively weak emission peak at 610 nm. This was due to the self-quenching effect of Ru(bpy)$_3$$^{2+}$. Due to its abundance in the clay, the individual molecules began to interact and quench each other. The ideal exposure concentration appears to be 1×10^{-3} M. At this concentration, the Ru(bpy)$_3$$^{2+}$ emission peak at 610 nm was more intense than at any other concentration (higher or lower) and the distorted baseline was virtually gone.

Comparing **Figure 3.5** to **Figure 3.1**, we see that the concentrations observed to generate the greatest emission intensity in solution did not correspond to those that

Comparing **Figure 3.5** to **Figure 3.1**, we see that the concentrations observed to generate the greatest emission intensity in solution did not correspond to those that generated the greatest intensity in the Zn-hectorite films. For example, the 1×10^{-4} M $Ru(bpy)_3^{2+}$ solution produced by far the greatest emission intensity of all the solutions. However, when the Zn-hectorite films were exposed to this solution, the $Ru(bpy)_3^{2+}$ emission intensity was not nearly as high as that of Zn-hectorite films exposed to 1×10^{-3} M $Ru(bpy)_3^{2+}$. The reason for this is that the concentration of the complex in the film was not the same in that in the solution. This effect intensified the $Ru(bpy)_3^{2+}$ emission peak for 1×10^{-3} M solution, because the concentration of the emitter in the film was then closer to the ideal 1×10^{-4} M concentration. However, it led to a decrease in the $Ru(bpy)_3^{2+}$ emission for 1×10^{-4} M solution because the new $Ru(bpy)_3^{2+}$ concentration in the sample was no longer 1×10^{-4} M.

The baseline effect can be explained by virtue of the fact that, the more concentrated solutions resulted in more fluorophore on the film to absorb the radiation from the 460 nm beam. This beam, therefore, was not reflected into the detector, but rather it was absorbed and used to excite the $Ru(bpy)_3^{2+}$. The lower concentration solutions did not provide the film with enough $Ru(bpy)_3^{2+}$ to absorb all of the 460 nm light. The excess was once again reflected into the detector and the baseline remained distorted.

3.1.6 Variation of Time of Zn-hectorite Film Exposure to $Ru(bpy)_3^{2+}$ Solution

Having established that the ideal cation to use to replace sodium in hectorite is Zn^{2+}, and the ideal concentration of $Ru(bpy)_3^{2+}$ solution for film exposure is 1×10^{-3} M, the only remaining variable in the production of the desired $Ru(bpy)_3^{2+}$/hectorite composite films was the amount of time to expose the film to $Ru(bpy)_3^{2+}$ solution.

Figure 3.6 shows the emission scans obtained from a study varying the amount of time that Zn-hectorite film was exposed to 1×10^{-3} M $Ru(bpy)_3^{2+}$ solution. The trend is very clear: the longer the exposure time, the lower the $Ru(bpy)_3^{2+}$ emission of the composite. For example, the 1 min exposure produced a very intense peak at 610 nm, while the 6 hour exposure produced almost no emission peak. This trend makes sense, because, as shown in **Figure 3.1**, the emission of 1×10^{-3} M $Ru(bpy)_3^{2+}$ solution was very minimal. The longer exposure times allowed more $Ru(bpy)_3^{2+}$ to migrate from the solution to the Zn-hectorite film, thus increasing the concentration of $Ru(bpy)_3^{2+}$ on the film, bringing it closer to the solution concentration. Therefore, more $Ru(bpy)_3^{2+}$—$Ru(bpy)_3^{2+}$ interactions (self-quenching) could occur and the emission signal decreased in intensity.

What, then, happens when the Zn-hectorite films are exposed to $Ru(bpy)_3^{2+}$ for only very small periods of time? **Figure 3.7** shows the results of such a study.

Figure 3.6: Emission scans of Zn-hectorite films exposed to 1×10^{-3} M Ru(bpy)$_3{}^{2+}$ solutions for varying lengths of time (ex $\lambda = 460$ nm)

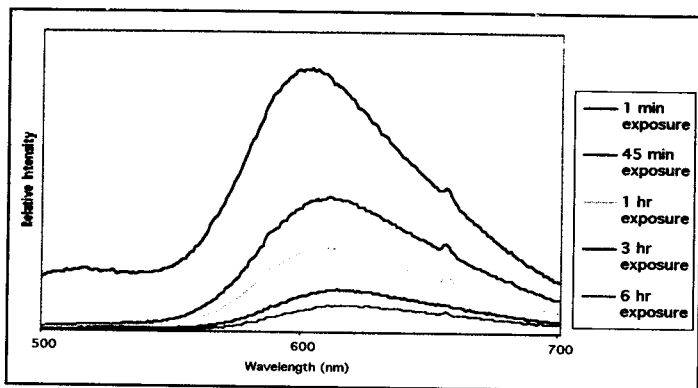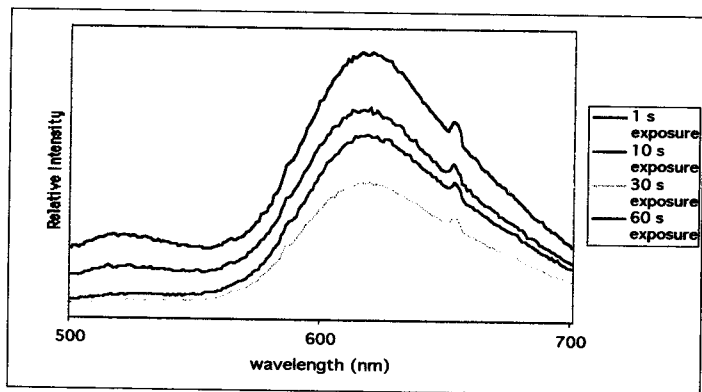**Figure 3.7**: Emission scans of Zn-hectorite films exposed to 1×10^{-3} M Ru(bpy)$_3{}^{2+}$ Solutions for varying lengths of time (ex $\lambda = 460$ nm)

There is really no clear trend exhibited in this situation. It is possible that there is no trend because it was very difficult to make accurate time measurements at such low levels. For example, it was very difficult to keep $Ru(bpy)_3^{2+}$ on the Zn-hectorite film for only 1 second. The $Ru(bpy)_3^{2+}$ had to be applied and then removed, a process that was nearly impossible to complete in 1 second. Another possibility for the irregularity is that the films used may not have been of the same thickness, thus varying the amount of $Ru(bpy)_3^{2+}$ that they could accomodate.

3.1.7 Variation of Excitation Wavelength in Fluorometric Studies

Ghosh[20] reported all emission data for an excitation wavelength of 460 nm. However, examination of the excitation spectrum of $Ru(bpy)_3^{2+}$-exchanged Zn-hectorite (**Figure 3.8**) indicated that this wavelength may not provide the maximum emission at 610 nm. This excitation scan displays peaks at 450, 463, 468, 473, and 481 nm, with the peak at 468 nm being the primary, most intense peak.

A preliminary study of the emission spectrum at these excitation wavelengths, as well as at 460 nm, is shown, in **Figure 3.9**, for a Zn-hectorite film exposed to 1×10^{-3} M $Ru(bpy)_3^{2+}$ for 1 minute. Clearly, the $Ru(bpy)_3^{2+}$/hectorite film gave a stronger emission peak when excited at 468 nm than when excited at 460 nm or any other wavelength. Further work is needed to verify the consistency of the fluorometric properties of the composites at this wavelength.

Figure 3.8: Excitation scan of Zn-hectorite film exposed to 1×10^{-3} M Ru(bpy)$_3^{2+}$ solution for 1 minute (em $\lambda = 610$ nm)
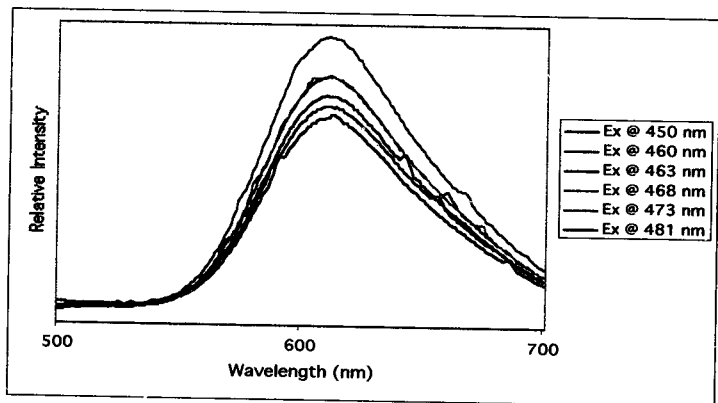

Figure 3.9: Emission scans of Zn-hectorite film exposed to 1×10^{-3} M Ru(bpy)$_3^{2+}$ Solutions for 1 minute (Varying ex λ)

The small peaks located at 565 nm and 656 nm when the samples were excited at 460 nm shifted to longer wavelengths as excitation wavelength increased. This verifies their Raman character.

3.2 X-Ray Diffraction

X-ray diffraction data have been collected that provide information about the incorporation of $Ru(bpy)_3^{2+}$ into the Zn-hectorite host framework. The data indicates intercalation of $Ru(bpy)_3^{2+}$ into the Zn-hectorite. MCM-41, a potential, mesoporous, alternative host, was also explored using XRD.

3.2.1 XRD Study of Water Intercalation

XRD can be used to verify that a substance has intercalated into the layered solids, like Zn-hectorite. The lamellar structure of ordered films shows a family of diffracted peaks representing (00l) planes of the host structure. These peaks are symmetry related and represent different slices of the unit cell. If intercalation has occurred, then the major peak of the Zn-hectorite spectrum, the (001) peak, should shift to a higher d-spacing (this is indicated by a leftward shift of the peak to a lower 2-theta angle). In order to verify that substances could intercalate and that the XRD instrument could detect the intercalation, we acquired an XRD spectrum for dry Zn-hectorite and very wet Zn-hectorite (See **Figure 3.10** and **Table 3.1**).

Table 3.1: Location and corresponding d-spacings of XRD peaks of dry and wet Zn-hectorite XRD Peaks

Dry Zn-hectorite		Wet Zn-hectorite	
Degrees 2-Theta	d-Spacing (Å)	Degrees 2-Theta	d-Spacing (Å)
7.67	13.37	4.64	22.11
16.32	6.30	9.04	11.35
---	---	20.34	5.07
22.24	4.64	22.41	4.64
31.88	3.26	31.42	3.30
33.93	3.07	33.93	3.07
35.75	2.91	35.75	2.91

Figure 3.10: XRD spectra of dry and wet Zn-hectorite

The data shows that the (001) Zn-hectorite peak corresponded to a d-spacing between layers of 13.37 Å. When the XRD pattern was collected on the wet sample, the peak shifted to a d-spacing of 22.11 Å. This was a d-space expansion of 8.74 Å. Clearly, the water intercalated into the clay structure. Therefore, the synthesized clay is capable of intercalation and the XRD instrument can verify this intercalation.

There is, however, a potential problem with the water intercalation. Because the exchange of $Ru(bpy)_3^{2+}$ into the clays requires film exposure to an aqueous solution of $Ru(bpy)_3^{2+}$, it is possible that evidence of water intercalation could be mistaken for evidence of $Ru(bpy)_3^{2+}$ intercalation. **Figure 3.11** and **Table 3.2** show the XRD pattern and data of the same Zn-hectorite film after it had redried.

It is evident from the data that, when the film dried completely, there was little to no evidence that the water had ever intercalated. The d-spacings all returned to within +/- 0.5 Å from where they were originally. Therefore, these samples can be safely used for $Ru(bpy)_3^{2+}$ analysis provided that they are sufficiently dried.

Figure 3.11: XRD spectra of a dry Zn-hectorite film (initial) and the same film after it has been exposed to water and then re-dried (later)

Table 3.2: Location and corresponding d-spacings of XRD peaks of initially dry Zn-hectorite and redried Zn-hectorite

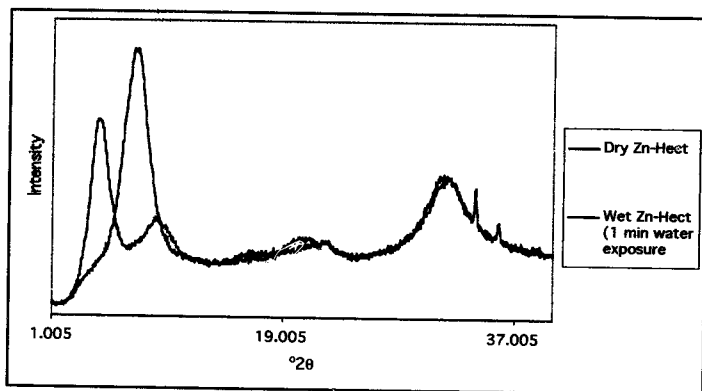| Initially Dry Zn-hectorite		Re-Dried Zn-hectorite	
Degrees 2-Theta	d-Spacing (Å)	Degrees 2-Theta	d-Spacing (Å)
7.67	13.37	7.45	13.78
16.32	6.30	16.48	6.24
22.24	4.64	22.17	4.65
31.88	3.26	32.64	3.18
33.93	3.07	33.93	3.07
35.75	2.91	35.75	2.91

There remains still another problem with the XRD of these films. The small peaks at 33.93 and 35.75 °2θ were too sharp and intense to be ignored, yet they were too irregular to be attributed to the (00l) family Zn-hectorite film peaks.

Figure 3.12: XRD spectra of Zn-hectorite film and Na-Hectorite powder

Table 3.3: Location and corresponding d-spacings of XRD peaks of a Zn-hectorite film and Na-hectorite powder

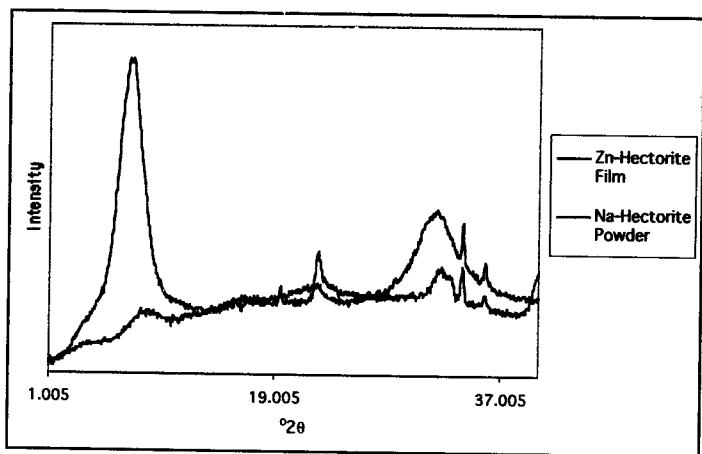| Zn-hectorite Film		Na-hectorite Powder	
Degrees 2-Theta	d-Spacing (Å)	Degrees 2-Theta	d-Spacing (Å)
7.67	13.37	8.66	11.85
16.32	6.30	19.43	5.30
22.24	4.64	22.39	4.61
31.88	3.26	32.33	3.21
33.93	3.07	33.93	3.07
35.75	2.91	35.76	2.92

Figure 3.12 and **Table 3.3** show the XRD data for the same Zn-hectorite film as in **Figures 3.10** and **3.11** and **Tables 3.1** and **3.2**, as well as for Na-hectorite powder (the powder that was exchanged with Zn^{2+} to make the Zn-hectorite films). Two of the major peaks in the XRD pattern of Na-hectorite powder are located at 33.93 and 35.76 °2θ. These corresponded almost exactly to the unidentifiable peaks found in the Zn-hectorite film's XRD pattern. Therefore, it can be concluded that the cause of these anomalous peaks was, in fact, the secondary phase of unexchanged Na-hectorite powder.

3.2.2 Variation of Time of Zn-hectorite Film Exposure to $Ru(bpy)_3^{2+}$ Solution

Having established from fluorometric data that the ideal conditions for composite formation were exposure of a Zn-hectorite film to 1×10^{-3} M $Ru(bpy)_3^{2+}$ solution for 1 minute, an XRD pattern was obtained for such a composite, after drying for 15 minutes. The XRD pattern and data for this film are shown in **Figure 3.13** and **Table 3.4**, respectively. The results show that there was very little intercalation at this level of $Ru(bpy)_3^{2+}$ exchange. Each of the peaks observed in the original, unexchanged, Zn-

There was, however, one significant difference. The (001) peak, located at 13.50 Å, developed a small shoulder at 17.32 Å. The formation of the shoulder indicates that some intercalation probably took place.

Figure 3.13: XRD spectra of a Zn-hectorite film and the same film exposed to 1 x 10^{-3} M Ru(bpy)$_3{}^{2+}$ solution for 1 minute

Table 3.4: Location and corresponding d-spacings of XRD peaks of a Zn-hectorite film and the same film exposed to 1 x 10^{-3} M Ru(bpy)$_3{}^{2+}$ solution for 1 minute

Zn-hectorite Film		Ru(bpy)$_3{}^{2+}$-Exchanged Zn-hectorite	
Degrees 2-Theta	d-Spacing (Å)	Degrees 2-Theta	d-Spacing (Å)
—	—	5.93	17.32
7.60	13.50	7.60	13.50
16.48	6.24	16.40	6.27
22.32	4.62	22.55	4.58
32.64	3.18	33.09	3.14
33.93	3.07	33.93	3.07
35.75	2.91	35.75	2.91

Figure 3.14: XRD spectra of a Zn-hectorite film and the same film exposed to 1×10^{-3} M Ru(bpy)$_3^{2+}$ solution for 1 hour

Since exposure of the Zn-hectorite film to 1×10^{-3} M Ru(bpy)$_3^{2+}$ produced evidence of possible intercalation, the same study was repeated. This time however, the exposure time was increased to 1 hour and the film was subsequently dried for 15 minutes. The XRD pattern and data for this study are shown in **Figure 3.14** and **Table 3.5**, respectively.

Table 3.5: Location and corresponding d-spacings of XRD peaks of a Zn-hectorite film and the same film exposed to 1 x 10^{-3} M Ru(bpy)$_3$$^{2+}$ solution for 1 hour
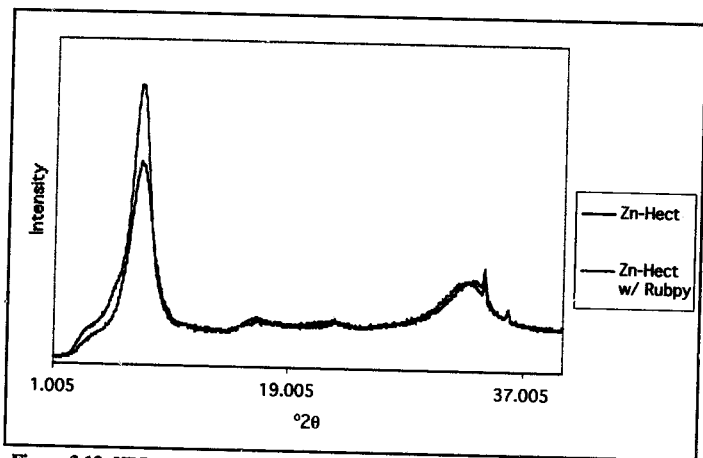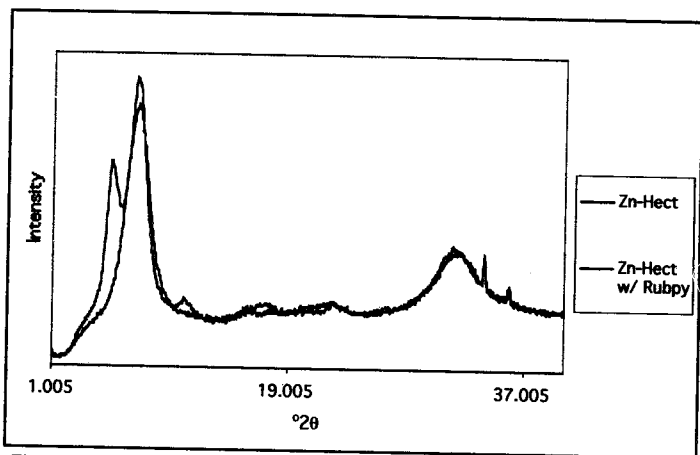
Zn-hectorite Film		Ru(bpy)$_3$$^{2+}$-Exchanged Zn-hectorite	
Degrees 2-Theta	d-Spacing (Å)	Degrees 2-Theta	d-Spacing (Å)
---	---	5.47	18.74
7.37	13.92	7.37	13.92
---	---	11.09	9.26
---	---	17.23	5.97
22.39	4.61	22.39	4.61
31.73	3.27	31.73	3.27
33.93	3.07	33.93	3.07
35.75	2.91	35.75	2.91

The data in **Figure 3.14** and **Table 3.5** show clear evidence of intercalation. A very distinct peak formed at 18.44 Å, which was a 4.82 Å expansion. Ru(bpy)$_3$$^{2+}$ has a diameter of 12.1 Å[7]. The inner gallery region of the clay is approximately 6 Å. The expansion makes the new size of the inner gallery region about 11 Å. Therefore, upon longer exposure time, the Ru(bpy)$_3$$^{2+}$ seemed to have intercalated into the film. It may have been intercalating into the gaps between the edges of the layers.

While the data in **Figure 3.11** and **Table 3.2** demonstrated that water should not have been the cause of the shift observed in **Figure 3.15** and **Table 3.6** provide further evidence for this. The XRD pattern was acquired on the same sample after drying for one week after the initial study.

Table 3.6: Location and corresponding d-spacings of XRD peaks of a Zn-hectorite film exposed to 1 x 10^{-3} M Ru(bpy)$_3$$^{2+}$ solution for 1 hour and the same film after drying for 1 week

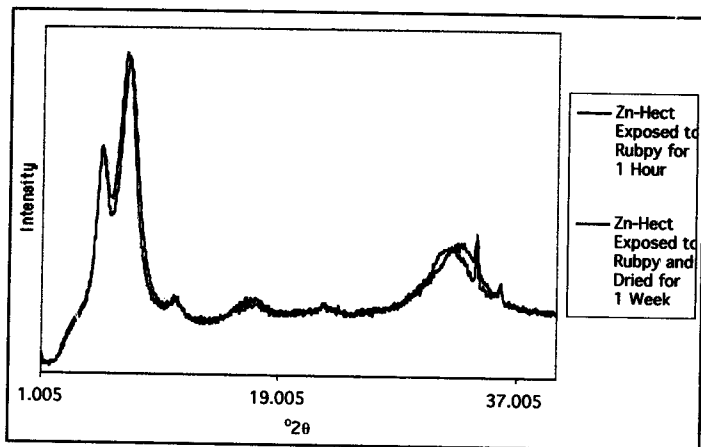| Dried for 15 Minutes		Dried for 1 Week	
Degrees 2-Theta	d-Spacing (Å)	Degrees 2-Theta	d-Spacing (Å)
5.47	18.74	5.47	18.74
7.37	13.92	7.52	13.64
11.09	9.26	11.09	9.26
17.23	5.97	17.23	5.97
22.39	4.61	22.39	4.61
31.73	3.27	32.64	3.18
33.93	3.07	33.93	3.07
35.75	2.91	35.75	2.91

Figure 3.15: XRD spectra of a Zn-hectorite film exposed to 1 x 10^{-3} M Ru(bpy)$_3^{2+}$ solution for 1 hour and the same film after drying for 1 week

Every peak from the initial composite of 1 hour Ru(bpy)$_3^{2+}$ exposure (that dried for 15 minutes) was accounted for in the XRD acquired after the sample that had dried for one week. Furthermore, each peak observed after a week of drying corresponded to a d-spacing within 0.3 Å of the initial composite. These data show clearly that the 15 minutes was a reasonable and valid drying time after the Zn-hectorite film was exposed to Ru(bpy)$_3^{2+}$. They also prove that the intercalation observed was caused by Ru(bpy)$_3^{2+}$ intercalation into the film, rather than water intercalation.

One hour exposure to Ru(bpy)$_3^{2+}$ solution appears to demonstrate intercalation. When a Zn-hectorite film was exposed to 1 x 10^{-3} M Ru(bpy)$_3^{2+}$ solution for 130 minutes, the intercalation became even more apparent. **Figure 3.16** and **Table 3.7** illustrate such a study.
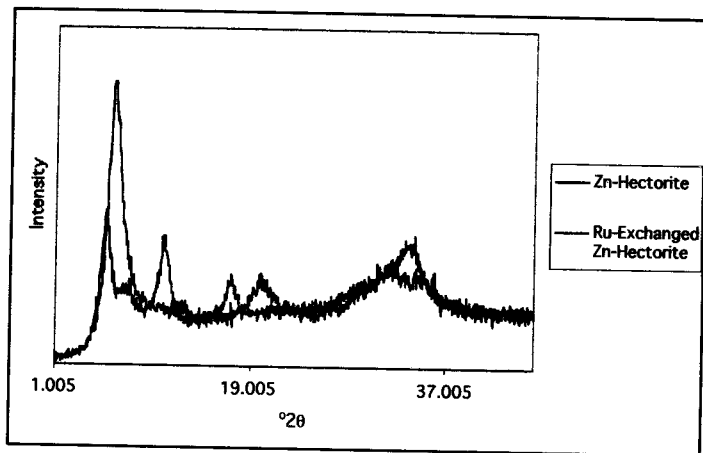
39

Figure 3.16: XRD's of a Zn-hectorite film and the same film exposed to 1 x 10⁻³ M Ru(bpy)₃²⁺ solution for 130 minutes

Table 3.7: Location and corresponding d-spacings of XRD peaks of a Zn-hectorite film and the same film exposed to 1 x 10⁻³ M Ru(bpy)₃²⁺ solution for 130 minutes

Zn-hectorite Film		Ru(bpy)₃²⁺-Exchanged Zn-hectorite	
Degrees 2-Theta	d-Spacing (Å)	Degrees 2-Theta	d-Spacing (Å)
6.33	16.21	5.56	18.45
---	---	7.52	13.64
12.05	8.52	11.02	9.31
19.90	5.18	17.17	5.99
33.90	3.07	31.68	3.28
35.86	2.91	35.86	2.91

These data show an even greater degree of intercalation than was observed for 1 hour exposure. A very distinct peak could be observed at 18.45 Å, which was a 4.81 Å expansion. This expansion was almost exactly the same as that observed for 1 hour Ru(bpy)₃²⁺ exposure. However, the major difference between the 1 hour exposure and the 130 minute exposure was that, for the 130 minute exposure, the primary Zn-hectorite

Ru(bpy)$_3$$^{2+}$ exposure. However, the major difference between the 1 hour exposure and the 130 minute exposure was that, for the 130 minute exposure, the primary Zn-hectorite peak, located at 16.21 Å, completely disappeared. Also, the (002) peak at 11.02 °2θ, which is absent in the host film, now shows appreciable diffraction in the composite film. The trend, therefore, was that increased exposure time of the Zn-hectorite films to 10^{-3} M Ru(bpy)$_3$$^{2+}$ solution resulted in increased levels of intercalation.

3.2.3 MCM-41

Zn-hectorite has been proven to be a good host material for Ru(bpy)$_3$$^{2+}$ in its potential applications to chemical sensing. However, other hosts may also be useful. We successfully carried out the synthesis of one such host, the mesoporous MCM-41, and the resulting XRD spectrum is given in **Figure 3.17**. The (001) peak was located at 2.40 °2θ.
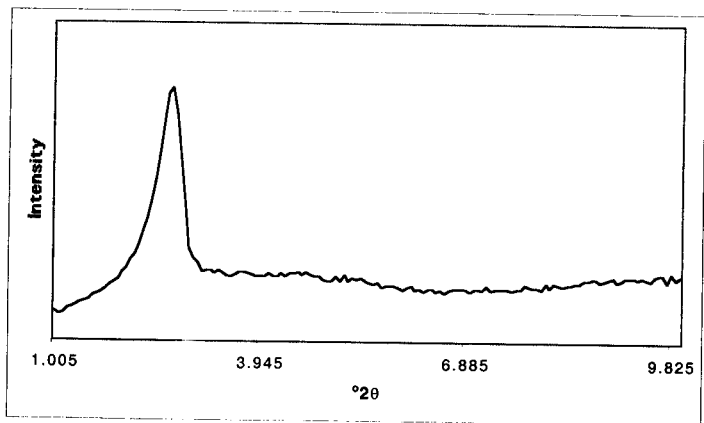

Figure 3.17: XRD spectrum of MCM-41 powder

41

The important characteristic of MCM-41 is that it has pore size (40 -100 Å) that is much larger than the intergallery region of hectorite clay. MCM-41 can, therefore, be used as a host material for molecules that are even bigger than $Ru(bpy)_3^{2+}$. However, MCM-41 does not cast thin films.

4. Conclusions

In summary, the results of this research have shown that the successful fabrication of $Ru(bpy)_3^{2+}$/hectorite composites is a delicate balance between maximizing $Ru(bpy)_3^{2+}$ exposure and keeping self-quenching to a minimum. Zn^{2+} has been found to be the ideal cation to exchange into Na-hectorite to produce thin films. These films could then be immersed in 1×10^{-3} M $Ru(bpy)_3^{2+}$ solution for 1 minute to achieve optimal emission intensity. While 460 nm has been the traditional excitation wavelength, this research has shown that 468 nm may, in fact, be a more optimal excitation wavelength.

While very short exposure times produced maximum emission intensity, they did not show significant levels of intercalation. Exposure for longer amounts of time, however, showed significant intercalation of the $Ru(bpy)_3^{2+}$ into the Zn-hectorite films. Therefore, there is a trade-off between emission intensity and level of intercalation.

Much research is still needed in this field. One important variable that was not controlled in this study is film thickness. Methods, such as spin coating, must be utilized to allow for controllable thickness. Casting the films directly onto supports (such as the fused quartz used in this research) may be a good starting point. However, once cast, the films are inseparable from the supports. This may be impractical for analysis, especially fluorometry. Further studies should be done to discover the exact loading capacity of the Zn-hectorite films and, thus, determine the concentration of $Ru(bpy)_3^{2+}$ in the films. Fluorescence lifetimes should be studied to characterize the ability of the composites to maintain the optical properties of $Ru(bpy)_3^{2+}$ for long lengths of time.

Further research should also be done using MCM-41 as a host. Unlike hectorite, this mesopore does not cast films well. However, its pores may be convenient loading sites for $Ru(bpy)_3^{2+}$ and even bigger molecules.

Continued study of polymerization on these films is needed. McManaman[21] performed an in depth study on the effects that hectorite films have on the polymerization of aniline and other similar monomers. However, there was no examination of a $Ru(bpy)_3^{2+}$/Zn-hectorite composite in this capacity.

The realization of solid film composites from hectorite exchanged with optically active $Ru(bpy)_3^{2+}$ is a logical first step toward the production of chemical sensors for oxygen, carbon dioxide, glucose, and possibly more. However, there is still much work to be done.

5. References

1. Ogawa, M.; Kuroda. K. *Chem. Rev.* **1995**, *95*, 399-438.

2. Pinnavaia, T.J. *Materials Chemistry*; American Chemical Society: Washington, DC, 1995, 283-300.

3. Giannelis, E. *Materials Chemistry An Emerging Discipline*; American Chemical Society: Washington, DC, 1995, 259-381.

4. Schöllhorn, R. *Chem Mater.* **1996**, *8*, 1747-1757.

5. Turbeville, W.; Robins, D.S.; Dutta P.K. *J. Phys. Chem.* **1992**, *96*, 5024-5029.

6. DeWilde, W.; Peeters, G.; Lunsford, J.H. *J. Phys. Chem.* **1980**, *84*, 2306-2310.

7. Lainé, P.; Lanz, M.; Calzaferri, G. *Inorg. Chem.* **1996**, *35*, 3514-3518.

8. Mallouk, T.E.; Gavin, J.A. *Acc. Chem. Res.* **1998**, *31*, 209-217.

9. Eastman, et al. *J. Electrochem. Soc.* **1991**, *138*, 1709.

10. Ferguson, G.S.; Kleinfeld, E.I. *Chem. Mater.* **1995**, *7*, 2327

11. Imisides, M.D.; John, R.; Wallace, G.G. *Chemtech.* **May 1996**, 19-25.

12. Ohsaka, T.; Yamaguchi, Y.; Oyama, N. *Bulletin of the Chemical Society of Japan* **1990**, *63*, 2646.

13. Lee, J.K.; Yoo, D.S.; Handy, E.S.; Rubner, M.F, *Appl Phys. Lett.* **1996**, *69*, 1686-1688.

14. Joshi, V.; Ghosh, P.K. *J. Am. Chem. Soc.* **1989**, *111*, 5604-5612.

15. Matsui, K.; Momose, F. *Chem. Mater.* **1997**, *9*, 2588-2591.

16. DellaGuardia, R.A.; Thomas, J.K. *J. Phys. Chem.* **1983**, *87*, 990-998.

17. Chang, R. *Chemistry, 5th Ed.*; McGraw-Hill: New York, 1994, 442.

18. Bragg, L. *The Crystalline State*; Cornell University Press: Ithaca, 1965.

19. Schoonheydt, R.A.; De Pauw, P.; Vliers, D.; De Schrijver, F.C. *J. Phys. Chem.* **1984**, *88*, 5113-5118.

20. Ghosh, P.K.; Bard, A.J. *J. Phys. Chem.* **1984**, *88*, 5519-5526

21. McManaman, C. *Union College* **1999.**

22. Wu, C.G.; Bein, Th. *Chem. Mater*. **1994**, *6*, 1109.

23. Beck, J.S.; Vartuli, J.C.; Roth, W.J.; Leonowicz, M.E.; Kresge, C.T.; Scmitt, K.D.; Chu, C.T-W.; Olson, D.H.; Sheppard, E.W.; McCullen, S.B.; Higgins, J.B.; Schlenker, J.L. *J. Am. Chem. Soc.* **1992**, *114*, 10834-10843.

24. Broomhead, J.A.; Young, C.G.; Hood, P. *Inorg. Synth.* **1971**, *29*, 127-128.

25. Eastman, M.P.; Bain, E.; Porter, T.L.; Manygoats, K.; Whitehorse, R.; Parnell, R.A.; Hagerman, M.E. *Applied Clay Science*, **1999**, *15*, 173-185.

26. Davis, M. *Microporous Matt.* **1993**, *2*, 1726